Journal of Applied Mechanics and Technical Physics, Vol. 46, No. 4, pp. 481–488, 2005

IMPULSIVE TENSION OF ETHANOL UNDER SHOCK LOADING

A. V. Utkin and V. A. Sosikov

UDC 532.538 + 539.593

This paper reports results from experimental studies of the strength of ethanol under impulsive tension due to interaction of a triangular compression pulse with the free surface. The experiments were performed in the range of strain rates $4 \cdot 10^4$–$4 \cdot 10^5$ sec^{-1}. It is established that the failure of ethanol is a two-stage process. In the first stage at a negative pressure of about 14 MPa, pore formation begins, which proceeds at a rather low rate and is manifested as an inflection on the free-surface velocity profile. In the second stage, the porosity growth rate increases, resulting in formation of a spalling pulse. The possibility of using the model of homogeneous nucleation to interpret experimental data is discussed.

Key words: *ethanol, cavitation, spalling, shock waves, impulsive tension.*

According to theoretical concepts, liquids can endure high tensile stresses of up to 0.1–1 GPa [1–3]. It is assumed that discontinuity of the material results from pore formation by a homogeneous nucleation mechanism. At the same time, considerably smaller values are observed [4] in practice under static test conditions, which is explained by the presence of heterogeneous centers in real liquids, at which pore growth is initiated.

Conditions of liquid fracture during homogeneous nucleation can be obtained using dynamic tension. In the present study, this is done by analyzing the spalling phenomena involved in the reflection of compression pulses from the free surface of the examined material [5]. An advantage of this method is that at a pulse duration of order of 1 μsec, the fracture is volume (with no effect of the boundaries) and occurs in a thin layer of the material, which considerably reduces the number of heterogeneous centers capable of influencing the fracture of the liquid. In addition, one might expect that precompression in a shock wave leads to partial pore collapse, which also enhances the role of homogeneous nucleation.

Impulsive tension under shock-wave loading has been used previously to study the cavitation of liquids (glycerol [6–9], water [10–13], ethylene glycol [11], ethanol [12], hexane [9] and mercury [14]). It has been shown, in particular, that the kinetics of pore formation and, as a consequence, the nature of the dependence of strength on strain rate are largely determined by the physicochemical properties of the liquids. To elucidate the general features of cavitation, it is of interest to compare the fracture patterns of liquids of various structures. The present paper considers the results of experiments on determining the spall strength of ethanol, which has not been studied previously, and discusses the possibility of using the homogeneous nucleation model to interpret the results obtained. Dremin et al. [12] obtained an estimate $P_s \approx 48$ MPa for the spall strength of ethanol, but the employed method did not allow regularities of the fracture kinetics to be established. This is one of the objectives of the present study.

Diagram and Results of Experiments. A diagram of the experiments on impulsive tension of liquids is presented in Fig. 1. Shock waves were produced by collision of an aluminum impactor (1) 0.2–2 mm thick accelerated by explosion products to a velocity of 500–600 m/sec with a Plexiglas dish bottom (shield 2) 2 mm thick. The loading conditions were varied by changing the thicknesses of the impactor h_{imp} and the liquid layer h_{liq} (3) and are listed in Table 1. The experiments performed under identical conditions are denoted by the same number, and only the results of the first of them are given in the figures. In experiment No. 3, the compression pulse was formed by direct action of explosion products on a copper screen 20 mm thick. The velocity was recorded by a VISAR

Institute of Problems of Chemical Physics, Russian Academy of Sciences, Chernogolovka 142432; utkin@icp.ac.ru; vaso@yandex.ru. Translated from Prikladnaya Mekhanika i Tekhnicheskaya Fizika, Vol. 46, No. 4, pp. 29–38, July–August, 2005. Original article submitted September 30, 2004.

TABLE 1

Experiment number	W_0, m/sec	P_0, MPa	h_{imp}, mm	h_{liq}, mm	ΔW, m/sec	P_{s0}, MPa	P_{sm}, MPa	P_s, MPa	$\dot{\varepsilon} \cdot 10^{-4}$, sec^{-1}
1	200	246	0.4	8	—	—	—	—	8.6
2	400	246	0.4	8	28	12.8	46	28.8	8.6
3	720	533	Cu	8	30	13.3	64	27.6	6.2
	722	535	Cu	8	27	12.4	60	26.6	4.5
4	269	360	0.4	4	—	—	—	—	17.2
5	544	365	0.4	4	32	14.7	50	32.5	17.2
6	766	581	0.4	1	33	15.1	15.1	15.1	38.6
	777	592	0.4	1	35	16	16	16.0	43.0
7	323	460	0.4	2	—	—	—	—	21.1
8	642	456	0.4	2	30	13.7	37	20.1	21.1
	650	464	0.4	2	29	13.3	36	19.5	20.5
9	899	730	2.0	8	20	9.2	—	30.2	17.4
	901	730	2.0	8	19	8.7	—	29.0	17.4

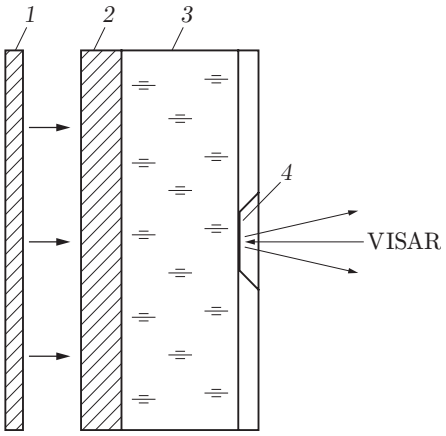

Fig. 1. Diagram of experiments on impulsive tension of liquids: 1) impactor; 2) shield; 3) liquid; 4) aluminum foil.

laser interferometer [15] with a constant of 80.8 m/sec, a measurement error of ±2 m/sec, and a time resolution of about 2 nsec. The laser beam was reflected from an aluminum foil 7 μm thick (4), which separated the liquid from air. The geometrical dimensions of the assembly (the diameter of the flat segment of the impactor was more than 40 mm) provided one-dimensional loading conditions and eliminated the arrival of the lateral rarefaction wave during the experiment. By the moment of arrival at the free surface, the compression pulse had the shape of a triangle, as was determined in separate experiments similar to those shown schematically in Fig. 1 but with the foil placed inside the liquid.

In the experiments, ethanol of density $\rho_0 = 0.786$ g/cm^3 at an initial temperature of 19°C was used and the sound velocity was $c_0 = 1.165$ km/sec. The mass velocity profiles plotted from the results of the experiments are given in Figs. 2–4. The compression-pulse amplitude P_0 was varied from 246 to 730 MPa, and the strain rate in the rarefaction part of the pulse $\dot{\varepsilon} = (dW/dt)/(2c_0)$ from $4.5 \cdot 10^4$ to $4.3 \cdot 10^5$ sec^{-1}. The maximum pressures were calculated by the generalized Hugoniot [16] $D = c_0 + 2u$ (u mass velocity), which is close to the Hugoniot proposed in [17] for $u < 2$ km/sec.

The arrival of the shock wave at the free surface causes a sudden increase in the velocity of the surface to a value W_0 equal to double the mass velocity in the shock wave. A centered rarefaction wave propagates inside ethanol and interacts with the incident rarefaction wave, leading to internal fracture — spalling. During fracture, the tensile stresses relax to zero to form a compression wave, which emerges as a spalling pulse from the free

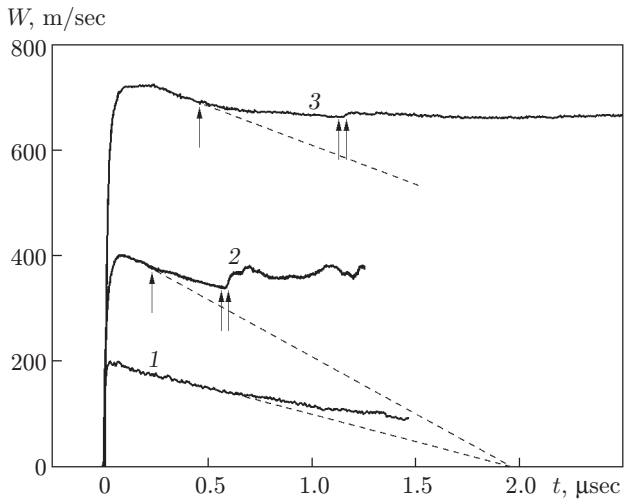

Fig. 2. Free-surface velocity profiles (2 and 3) and mass-velocity profile (1) in experiment No. 2 (the dashed curves are extrapolations of the free-surface velocity in the absence of cavitation).

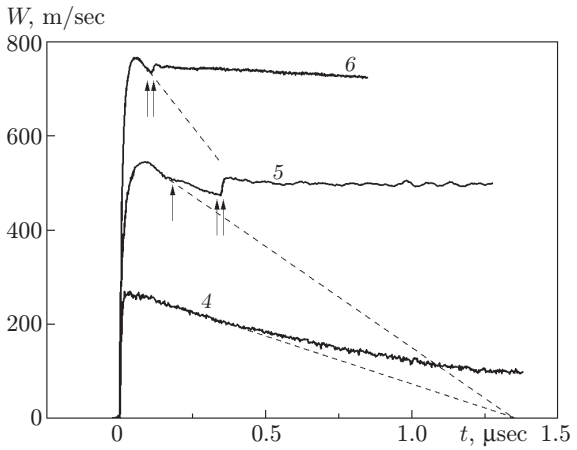

Fig. 3

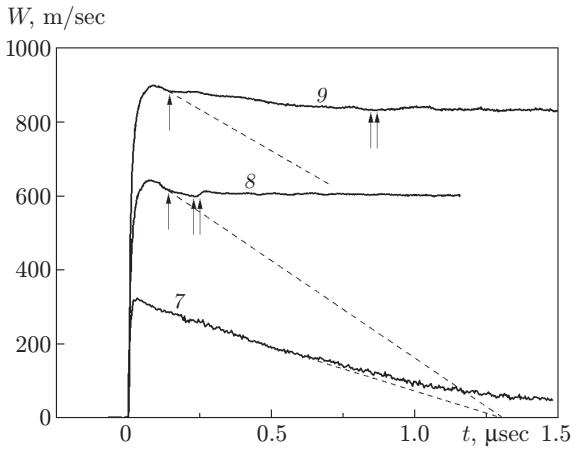

Fig. 4

Fig. 3. Free-surface velocity profiles (5 and 6) and mass-velocity profile (4) in experiment No. 5 (the dashed curves are extrapolations of the free-surface velocity in the absence of cavitation).

Fig. 4. Free-surface velocity profiles (8 and 9) and mass-velocity profile (7) in experiment No. 8 (the dashed curves are extrapolations of the free-surface velocity in the absence of cavitation).

surface. The indicated features are observed on the velocity profiles given in Figs. 2–4. Mass velocities in the incident compression pulses were measured in experiment Nos. 1, 4, and 7, and their corresponding free-surface velocities in experiment Nos. 2, 5, and 8. A comparison of these profiles shows that the velocity-doubling rule is satisfied with good accuracy. This confirms the absence of cavitation on the foil–ethanol boundary, which would lead to a decrease in the cohesion between the foil and ethanol and, as a consequence, to a decrease in the velocity slope immediately after the arrival of the shock wave at the free surface. The dashed curves in Figs. 2–4 show how the free-surface velocity would vary in the absence of fracture.

Measurements of the incident-pulse parameters allow one to uniquely determine the effect of the fracture kinetics on rarefaction. For example, in the phase of decreasing free-surface velocity (experiment No. 3), an inflection (denoted in Fig. 2 by a vertical arrow) is recorded in approximately 0.25 μsec after the arrival of the shock wave. Similar features are due to the shape of the initial pulse or cavitation. A comparison of profiles 1 and 2 shows that the incident compression pulse does not have an inflection in the neighborhood of 0.25 μsec; therefore, its occurrence

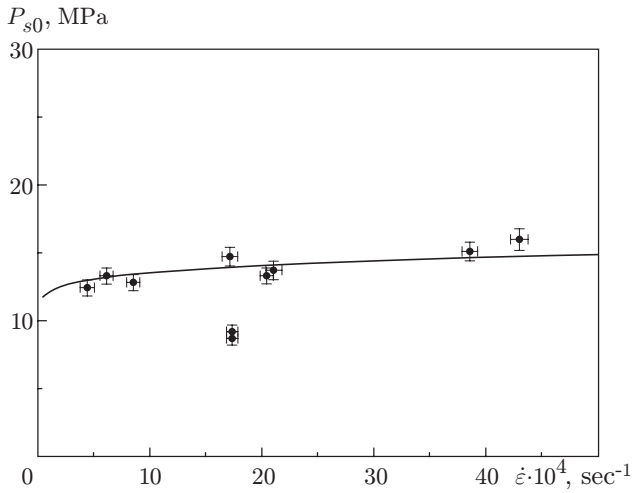

Fig. 5. Fracture initiation threshold versus strain rate: the points refer to experiment and curves to calculation.

on the free-surface velocity profile is due to the pore-growth kinetics. Moreover, a similar inflection was observed in all experiments (except in experiment No. 6), and its corresponding negative pressure P_{s0} should be treated as the fracture initiation threshold, which is determined from the free-surface velocity W_{s0} at the inflection point [5]:

$$P_{s0} = 0.5\rho_0 c_0 \, \Delta W, \tag{1}$$

where $\Delta W = W_0 - W_{s0}$. The cross section at which it is reached is equal to half the product of c_0 by the time of occurrence of the inflection and, for example, in experiment No. 3, it is at 150 μm from the free surface.

The fracture initiation threshold calculated in such a manner is given in Table 1 and Fig. 5 as a curve of $P_{s0}(\dot{\varepsilon})$. It is evident that P_{s0} is almost constant in the entire range of strain rates and is equal to (14.5 ± 1.5) MPa. The exception is experiment No. 9, in which the shock-wave amplitude was maximal before the arrival at the free surface and this was apparently responsible for a sharp, more than a factor of 1.5, decrease in the cavitation threshold.

After the beginning of cavitation, the negative pressures continue to increase inside the liquid as the rarefaction wave reflected from the free surface propagates into the depth of the sample. In this case, volume fracture occurs rather slowly and shows up on the velocity profile as a decrease in the absolute value of the velocity gradient behind the inflection point [18, 19] rather than as a spalling pulse. This proceeds until the pore growth rate exceeds a certain critical value [18], which leads to the formation of a spalling pulse. In Figs. 2–4, the time of arrival of the spalling pulse on the free surface is denoted by two arrows. The variation in the time dependence of the free-surface velocity due to variation in the shock-wave amplitude follows a definite law. As the shock-wave amplitude becomes larger, the deviation of the velocity profile from the dashed curve increases and, simultaneously, the spalling pulse approaches the inflection point up to their coincidence in experiment No. 6. A further increase in the amplitude (experiment No. 9) leads to degeneration of the spalling pulse into a horizontal line, followed by an almost monotonic decrease in the velocity. Therefore, the singularities indicated by arrows on profile 9 are rather conditional. We note that the maximum negative pressures occurring in ethanol can notably exceed the fracture initiation threshold P_{s0}, but to determine them, one needs to propose a particular mechanism for the porosity growth in the sample.

Previously, experiments in a similar formulation have been performed to record negative pressures in water [13], hexane, and glycerol [9]. The free-surface velocity profiles obtained for these liquids are qualitatively similar to those given in Figs. 2–4 for ethanol but the initial fracture rate was so high that spalling-pulse formation coincided with fracture initiation within the experimental error. Therefore, a two-stage nature of fracture, which first leads to inflection of the velocity profile and only then, after a rather considerable time, to spalling-pulse formation, has not been observed in previous studies. The spalling-pulse front in ethanol, especially at low pressures, is very abrupt (for example, in experiment No. 5, its characteristic time is about 10 nsec), and the subsequent velocity oscillations due to wave circulation between the sample surface and the fracture region are not observed. This is likely related

to the absence of sharp boundaries of the cavitation zone, because of which the notion of the spall-plate thickness becomes rather conditional. In the respect, the cavitation-development processes in ethanol and water are very similar [13].

Discussion of Experimental Results. At negative pressures that occur in the case of impulsive tension, the liquid enters the region of a metastable state, whose lifetime is determined by both the purity of the liquid and tension conditions. In the experiments performed, ethanol was first compressed in the shock wave to the maximum pressure P_0 indicated in Table 1 and was then unloaded isentropically to the states corresponding to the points lying below the liquid–vapor equilibrium curve. Failure of the metastable state occurs only by growth of pores, both those that exist stably in the liquid and those generated by thermal fluctuations. Bogach and Utkin [13] showed that the pores existing in the liquid do not affect the initiation of the cavitation process and that the experimental weak dependence of P_s on the strain rate for water is explained by the process of homogeneous nucleation.

Let us consider the effect of homogeneous nucleation on the porosity increase in the case of spalling in ethanol. According to thermodynamic fluctuation theory [1, 20], the number of pores of the critical radius R_c formed per unit volume in unit time J under negative pressure P is described by the kinetic equation

$$J = N_0 \frac{\sigma}{\eta} \sqrt{\frac{\sigma}{kT}} \exp\Big(- \frac{16\pi\sigma^3}{3P^2kT}\Big), \tag{2}$$

where N_0 is the number of molecules per unit volume of the liquid, σ is the surface tension, η is the viscosity, T [K] is the temperature, and k is Boltzmann's constant. From Figs. 2–4, it is evident that after the fracture initiation, the absolute value of the velocity gradient in the rarefaction part of the pulse decreases severalfold. Investigation of the effect of the pore-growth kinetics on the dynamics of wave interactions during spallation shows [21] that this is possible if the porosity growth rate, which is proportional to $R_c^3 J$ [13], exceeds a certain critical value dependent on the strain rate in the rarefaction part of the incident pulse: $R_c^3 J = \gamma\dot{\varepsilon}$, where $\gamma \sim 1$.

Assuming that the tough growth of pores, i.e., the nucleation process described by relation (2), is the determining process for the porosity growth, it is possible to find the dependence of the fracture initiation threshold on the strain rate [21]:

$$P_{s0} \approx A/\sqrt{\ln(B/\dot{\varepsilon})}. \tag{3}$$

Here A and B are constants that depend on temperature both explicitly and via viscosity and surface tension. In Fig. 5, relation (3) plotted for $A = 41$ MPa and $B = 10^{11}$ sec^{-1} is shown by a solid curve and can be seen to describe experimental data well. The exception is experiment No. 9, in which a marked deviation from relation (3) is observed. We note that a decrease in the strength with increase in the shock-wave amplitude was earlier observed for water in [13], where it was noted that within the framework of homogeneous nucleation, this cannot be explained by an increase in residual temperature. It is probable that a rise in pressure enhances the role of the local heating of the pores existing in the liquid, resulting in formation of hot spots. Therefore, at the moment of occurrence of tensile stresses, there may be regions in the liquid with temperature above residual temperature, in which homogeneous nucleation proceeds at the highest rate. Probably, at high pressures, a similar hot-spot fracture mechanism also occurs in ethanol.

We now attempt to estimate the maximum negative pressures in ethanol. This is easy to do assuming that the initial fracture rate is equal to zero. Then, as shown in [21], the maximum negative pressures P_{sm} occur behind the rarefaction-wave front reflected from the free surface (the flow is considered in an acoustic approximation; therefore, the rarefaction wave front does not decrease) and has the same value as in the intact sample. The value of P_{sm} is calculated by formula (1) but instead of W_{s0} we use the free-surface velocity value W_{sm} that would be reached in front of the spalling pulse if there was no inflection on the free-surface velocity profile. In Figs. 2–4, these points lie on the dashed straight lines, which are continuations of the velocity profile in the absence of fracture, directly under the real velocity minima denoted by two arrows. The corresponding state changes in the variables t and h (h is the Lagrangian coordinate) and P and u (u is the mass velocity) are shown in Figs. 6 and 7, respectively. In region I in Fig. 6, the flow is determined by the initial compression pulse. In region III, there is interaction between the incident rarefaction wave (C_+-characteristics) and the rarefaction waves reflected from the free surface (C_--characteristics) but the fracture initiation threshold is not yet reached; fracture starts at the point $(\tau_{s0}, -h_{s0})$ and proceeds in region II. Let the minimum of the free-surface velocity occur when the C_+ characteristic $ABCD$ arrives at the free surface. On the plane P–u (Fig. 7), the states in the incident wave lie on the straight line ON. If

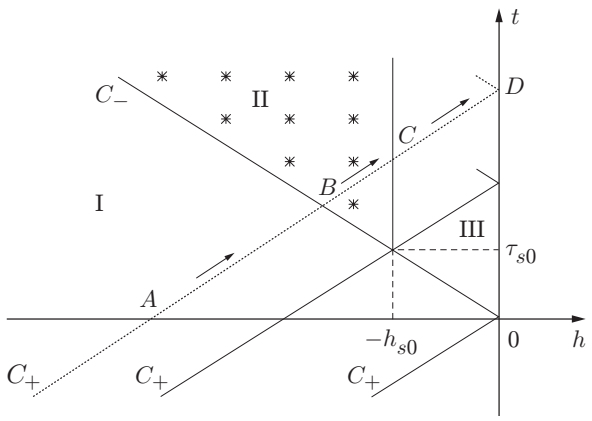

Fig. 6

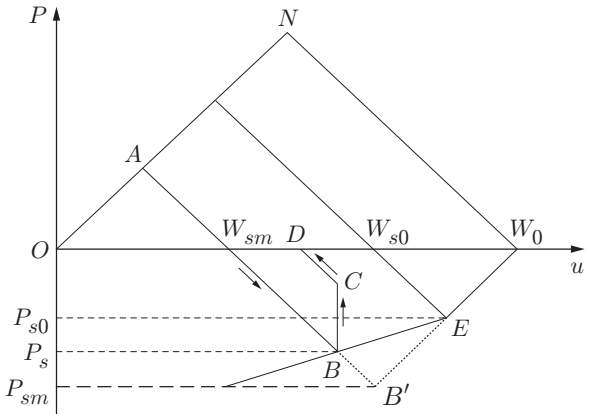

Fig. 7

Fig. 6. Variation in the state of ethanol in the time–Lagrangian coordinate plane.

Fig. 7. Variation in the state of ethanol in the pressure–mass velocity plane.

the initial fracture rate is equal to zero, then after meeting the leading C_- characteristic of the reflected rarefaction wave, the state passes suddenly from the point A to the point B', which determines the maximum tensile stress P_{sm} along this C_+-characteristic. The further change of the state from the point B' to the point C depends on the particular fracture kinetics and is not indicated in the figure. The thus obtained values of P_{sm} are listed in Table 1, and, as can be seen, they are several time higher than P_{s0} and vary in the interval 40–60 MPa. The exception is experiment No. 6, in which the inflection point coincides with the spalling pulse ($P_{sm} = P_{s0}$), and experiment No. 9, in which the spalling pulse is hardly observed and the maximum tensile stresses are not determined because of a great arbitrariness in the estimate of P_{sm}. We note that the obtained strength of ethanol (50 ± 10) GPa coincides with the result of [12], where the maximum tensile stresses were evaluated from the spall-plate thickness.

A more realistic estimate of the negative pressures can be obtained assuming that the fracture rate is constant, which is supported by the nearly linear time dependence of the free-surface velocity behind the inflection point [18]. In this case, the free-surface velocity gradient after fracture initiation is defined by the relation [18]

$$\frac{dW}{dt} = \frac{W_0}{8\tau_0}\Big(\frac{\dot V_p}{\dot V} - 4\Big),$$

where τ_0 is the duration of the compression pulse, which is considered triangular, $\dot V_p$ is the fracture rate (the rate of increase in the specific pore volume), and $\dot V$ is the dilatation rate of the material in the rarefaction part of the incident pulse. For definiteness and simplicity, we assume that after fracture initiation, the absolute value of velocity gradient decreases by a factor of two, i.e., $\dot V_p = 2\dot V$ In this case, entering the fracture region, the trajectory of state variation along the C_- characteristics in the plane P–u undergoes an inflection at the point $(\tau_{s0}, -h_{s0})$ and the derivative dP/du decreases by a factor of three (the trajectory W_0EB in Fig. 7) [18].

The state variation along the C_+ characteristics in the plane P–u is shown in Fig. 7 by arrows. After meeting the leading characteristic of the rarefaction wave, the state passes suddenly from the point A to the point B and varies along the trajectory BC in the fracture region (the velocity of the material remains unchanged and the pressure increases). On the segment CD in the intact part of the sample, the slope of the characteristic is equal to $-\rho_0 c_0$. At the point D, the free-surface velocity reaches a minimum, and the maximum tensile stress P_s occurs at the point B and is equal to

$$P_s = (P_{s0} + P_{sm})/2.$$

The obtained relation is a direct consequence of the assumption of a factor of two decrease in the velocity gradient after sample fracture initiation and gives the same estimate of P_s as calculations by formula (1) if instead of W_{s0} one uses the free-surface velocity W_s reached before the spalling pulse. This conclusion remains valid for any value of the constant fracture rate, which allows the tensile stresses P_s to be calculated directly by formula (1). The values obtained are listed in Table 1.

Ignoring experiment Nos. 6 and 8, we have $P_s = (30 \pm 3)$ MPa. The sharp decrease in the maximum tensile stresses in experiment Nos. 6 and 8 cannot be explained only by an increase in the shock-wave amplitude, because, for example, in experiment Nos. 3 and 9, the shock pressure is nearly the same whereas P_s is much higher. At the same time, in experiment Nos. 6 and 8 there was not only a large shock-wave amplitude but also the maximum strain rate in excess of $2 \cdot 10^5$ sec^{-1}. That is, the decrease in P_s is due to an increase in both the pressure and strain rate. In experiment No. 9, the strain rate $\dot{\varepsilon}$ is also near the critical value, but, as was noted above, the spalling pulse is not well-defined and P_s is determined with a large error. Moreover, the nature of variation in the free-surface velocity in this experiment is identical to that in the case of tough fracture [19], where the porosity increase is due to pore growth rather than to pore formation by homogeneous nucleation. In [19], it is shown that if the toughness exceeds a certain threshold value (dependent, in particular, on the strain rate), the spalling pulse disappears and the free-surface velocity decreases monotonically, as was observed in experiment No. 9. Therefore, unlike for the fracture initiation threshold P_{s0}, whose dependence on the strain rate is determined by the homogeneous nucleation mechanism, there is no unambiguous explanation for the nature of variation in the maximum tensile stresses P_s with increase in the shock-wave amplitude and strain rate. The main reason for this is apparently the possibility of change in the kinetics of porosity formation, i.e., in the second stage of fracture, it is necessary to allow for not only pore formation but also pore growth.

Thus, in contrast to the previously studied liquids, the fracture of ethanol is a two-stage process. In the first stage at negative pressures of about 14 MPa, pore formation begins, which proceeds at a slow velocity and is manifested as an inflection on the free-surface velocity profile. In the second stage, the porosity growth rate becomes higher, leading to formation of a spalling pulse. The homogeneous nucleation model explains the experimental weak dependence of the fracture initiation threshold on the strain rate for of ethanol.

REFERENCES

1. Ya. B. Zel'dovich, "On the theory of new phase formation. Cavitation," *Zh. Éksp. Teor. Fiz.*, **12**, Nos. 11/12, 525–538 (1942).
2. J. C. Fisher, "The fracture of liquids," *J. Appl. Phys.*, **19**, 1062–1067 (1948).
3. M. Kornfel'd, *Elasticity and Strength of Liquids* [in Russian], Gostekhteoretizdat, Moscow–Leningrad (1951).
4. V. P. Skripov, *Metastable Liquid* [in Russian], Nauka, Moscow (1972).
5. G. I. Kanel', S. V. Razorenov, A. V. Utkin, and V. E. Fortov, *Shock-Wave Phenomena in Condensed Media* [in Russian], Yanus, Moscow (1996).
6. D. C. Erlich, D. C. Wooten, and R. C. Crewdson, "Dynamic tensile fracture of glycerol," *J. Appl. Phys.*, **42**, No. 13, 5495–5502 (1971).
7. G. A. Carlson and K. W. Henry, "Technique for studying dynamic tensile in liquids: Application to glycerol," *J. Appl. Phys.*, **44**, No. 5, 2201–2206 (1973).
8. G. A. Carlson and H. S. Levine, "Dynamic tensile strength of glycerol," *J. Appl. Phys.*, **46**, No. 4, 1594–1601 (1975).
9. A. V. Utkin, V. A. Sosikov, and A. A. Bogach, "Impulsive tension of hexane and glycerol under shock-wave loading," *J. Appl. Mech. Tech. Phys.*, **44**, No. 2, 174–180 (2003).
10. P. L. Marston and G. L. Pullen, "Cavitation in water induced by the reflection of shock waves," in: *Proc. Conf. of the Amer. Phys. Soc. on Shock Waves in Condensed Mater* (Merlo Park, California, USA, June 23–25, 1981), AIP, New York (1982), pp. 515–519.
11. P. L. Marston and B. T. Urgen, "Rapid cavitation induced by the reflection of shock waves," in: *Proc. Con of the Amer. Phys. Soc. on Shock Waves in Condensed Mater* (Spokane, Washington, USA, July 22–25, 1985), Plenum Press, New York (1986), pp. 401–405.
12. A. N. Dremin, G. I. Kanel', and S. A. Koldunov, "Spalling in water, ethanol, and Plexiglas, in: *Combustion and Explosion*, Proc. III All-Union Symp. on Combustion and Explosion (Leningrad, July 5–10, 1972), Nauka, Moscow (1972), pp. 569–574.
13. A. A. Bogach and A. V. Utkin, "Strength of water under pulsed loading," *J. Appl. Mech. Tech. Phys.*, **41**, No. 4, 752–759 (2000).
14. G. A. Carlson, "Dynamic tensile strength of mercury," *J. Appl. Phys.*, **46**, No. 9, 4069–4070 (1975).

15. J. R. Asay and L. M. Barker, "Interferometric measurement of shock-induced internal particle velocity and spatial variations of particle velocity," *J. Appl. Phys.*, **45**, No. 6, 2540–2546 (1974).
16. A. N. Afanasenkov, V. M. Bogomolov, and I. M. Voskoboinikov, "Generalized Hugoniot of condensed materials," *Prikl. Mekh. Tekh. Fiz.*, No. 4, 137–141 (1969).
17. R. F. Trunin, L. F. Gudarenko, M. V. Zhernokletov, and G. V. Simakov, *Experimental Data on Shock-Wave Compression and Adiabatic Tension of Condensed Materials* [in Russian], Institute of Experimental Physics, Sarov (2001).
18. A. V. Utkin, "Effect of initial failure rate on the formation of a spalling pulse," *J. Appl. Mech. Tech. Phys.*, **34**, No. 4, 578–584 (1993).
19. A. V. Utkin, "Effect of fracture rate on the dynamics of the interaction of an impact load pulse with the surface of a solid," *J. Appl. Mech. Tech. Phys.*, **33**, No. 6, 729–735 (1992).
20. Yu. Kagan, "Boiling kinetics of a pure liquid," *Zh. Fiz., Khim.*, **34**, No. 1, 92–101 (1960).
21. A. V. Utkin, "Determination of the constants of spall-fracture kinetics of materials using experimental data," *J. Appl. Mech. Tech. Phys.*, **38**, No. 6, 952–961 (1997).